

# Pseudo 3D Perception Transformer with Multi-level Confidence Optimization for Visual Commonsense Reasoning

Jian Zhu, and Hanli Wang, *Senior Member, IEEE*,

**Abstract**—A framework performing Visual Commonsense Reasoning (VCR) needs to choose an answer and further provide a rationale justifying based on the given image and question, where the image contains all the facts for reasoning and requires to be sufficiently understood. Previous methods use a detector applied on the image to obtain a set of visual objects without considering the exact positions of them in the scene, which is inadequate for properly understanding spatial and semantic relationships between objects. In addition, VCR samples are quite diverse, and parameters of the framework tend to be trained suboptimally based on mini-batches. To address above challenges, pseudo 3D perception Transformer with multi-level confidence optimization named PPTMCO is proposed for VCR in this paper. Specifically, image depth is introduced to represent pseudo 3-dimension (3D) positions of objects along with 2-dimension (2D) coordinates in the image and further enhance visual features. Then, considering that relationships between objects are influenced by depth, depth-aware Transformer is proposed to do attention mechanism guided by depth differences from answer words and objects to objects, where each word is tagged with pseudo depth value according to related objects. To better optimize parameters of the framework, a model parameter estimation method is further proposed to weightedly integrate parameters optimized by mini-batches based on multi-level reasoning confidence. Experiments on the benchmark VCR dataset demonstrate the proposed framework performs better against the state-of-the-art approaches.

**Index Terms**—Visual commonsense reasoning, pseudo 3D perception, transformer, multi-level confidence optimization.

## I. INTRODUCTION

In recently years, with the rapid growth of the available vision-and-language data volume, many challenging tasks have been studied to analyze these data such as referring expressions [1], [2], image and video captioning [3], [4], visual question answering (VQA) [5], [6] and visual commonsense reasoning (VCR) [7], [8]. These tasks all require the cross-modal intelligence to not only recognize entities in data but also understand their intrinsic interactions in varying degrees. For instance, referring expressions is to localize the entities described by the language in the image, where cross-modal associations are primarily considered. VCR is a reasoning task to choose an answer and further provide a rationale justifying based on the given image and question. In such a task, the

cross-modal intelligence also need to model discriminative intra-modal associations for reasoning, and VCR is promising in many fields such as robot dialogue system, private virtual assistant and baby development assistance.

To tackle the challenging VCR task, various approaches have been adopted to analyze the complicated and associated data in VCR. Many frameworks adopted multi-branch models to independently associate the cross-modal data, and fuse features obtained for reasoning later [7]–[9]. For instance, Zeller *et al.* [7] used LSTM and attention mechanism to contextualize the answer with the image or the question. Yu *et al.* [9] constructed heterogeneous graphs to model correlations between different domains. Zhang *et al.* [8] associated structured syntactic triplets of different sentences with the visual graphs for reasoning. In the VCR task, the image contains all the facts that can be leveraged to do reasoning. Therefore, extracting discriminative visual features and properly associating them with languages are crucial. Lin *et al.* [10] adopted an object detector integrating attributes such as colors, texture, size to enhance visual features for VCR, and some works following also used such an enhanced detector [8], [11].

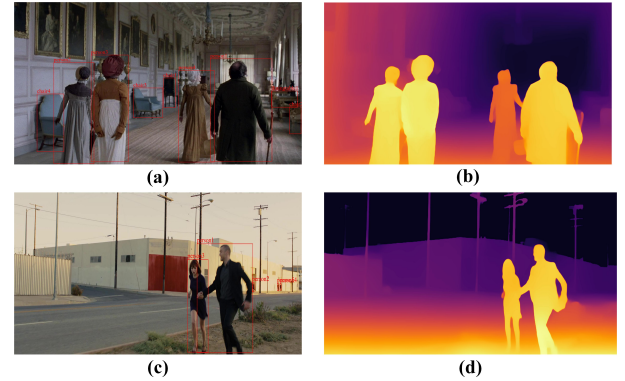


Fig. 1. Examples of RGB images (left) and depth images (right) generated from them. In depth images, the pixel appears from yellow to black as the distance becomes farther. With the help of image depth, the framework can represent objects in a way closer to human’s visual perception.

In general, all methods mentioned above utilized various detectors to obtain a set of objects for further processing without considering the exact positions of objects in the scene, which are crucial to understanding spatial and semantic relationships between objects. Intuitively, 2-dimension (2D) coordinates of objects obtained by an object detector can be used to represent positions of objects in the image, which is

*Corresponding author: Hanli Wang.*

J. Zhu and H. Wang are with the Department of Computer Science & Technology, Key Laboratory of Embedded System and Service Computing (Ministry of Education), Tongji University, Shanghai 200092, P. R. China, and with Frontiers Science Center for Intelligent Autonomous Systems, Shanghai 201210, P. R. China (e-mail: jianzhu@tongji.edu.cn, hanliwang@tongji.edu.cn).

still insufficient for correct representation nevertheless. As is shown in Fig. 1(a), "person 4" is close to "chair 1" with regard to the 2D coordinates in the image. However, an object need typically a set of 3-dimension (3D) coordinates to completely represent the position in the real world. Compared with the 2D coordinates in the image, there is an additional dimension measuring the distance from the object to the image plane in the 3D coordinates, which can be converted to image depth [12]. Recently, with the development of monocular depth estimation [12], image depth can be easily obtained from a monocular RGB image. Fig 1(b) is the depth image generated from Fig 1(a), which reflects that "person 4" is actually far away from "chair 1" with image depth considered. In addition, it can be observed in Fig 1(c) and (d) that objects with similar depth values (e.g. "person 1" and "person 3") are more likely to have close relationships (e.g. "person 1" holds the hand of "person 1"), especially in the foreground of the image. With image depth introduced, the model owns more characteristics of human's visual perception since different distances can be distinguished and the visual field becomes smaller as the distance is shorter. Therefore, image depth which is usually ignored in image understanding can be of benefit to exactly describing objects and analyzing associations between them.

VCR is a challenging reasoning task, where the image needs to be understood as precisely as possible to provide the reasoning rationale. Inspiring by analyzing the image in a way closer to human's visual perception, pseudo 3D perception Transformer with multi-level confidence optimization named PPTMCO for VCR is proposed in this paper. The framework uses a two-branch Transformer [13] architecture to independently associate the answer with the image or the question, and combine results of branches for further reasoning. In the stage of image processing, visual features of objects detected are enhanced by pseudo 3D positions and features of depth image regions. In the answer-image branch, depth-aware Transformer (DT) is proposed which uses depth differences to guide attention mechanism from words and objects to objects. Words of each answers are also tagged with pseudo depth values according to related objects. Since samples of VCR usually vary from each other and are difficulty to be fit, a model parameter estimation method guided by multi-level reasoning confidence (PSMRC) is further proposed to weightedly integrate parameters of models optimized by mini-batches to obtain better parameter values.

In summary, the major contributions of this work are the following three-folds: (1) Image depth is firstly investigated in the cross-modal reasoning task by enhancing object features and guiding depth-aware attention in a way closer to human's visual perception. (2) A model parameter estimation method is proposed to relieve sub-optimization caused by diverse samples via weightedly integrating parameters based on multi-level reasoning confidence. (3) The proposed framework achieves new state-of-the-art results on the VCR benchmark dataset, demonstrating the effectiveness of the approach.

## II. RELATED WORK

### A. Visual Commonsense Reasoning

Visual commonsense reasoning (VCR) is a reasoning task to choose an answer and further provide a rationale justifying based on the given image and question. A main difficulty of VCR is how to sufficiently and properly represent visual cues from the image and associate them with linguistic data for reasoning. Previous methods can be roughly divided into two categories: (1) explore models processing sequential data, (2) adopt graph-based networks. At the earliest, Zeller *et al.* [7] used LSTM with attention mechanism to contextualize sequential answer words with sequential question words or visual objects. Later, Lin *et al.* [10] integrated attributions of objects such as color and texture to enhance visual features used in [7]. Wen *et al.* [14] adopted an additional linguistic knowledge base to transfer commonsense knowledge to the LSTM model doing VCR. Su *et al.* [15] used cross-modal sequential data consisting of visual objects and linguistic words from several cross-modal datasets to train BERT model, then fine-tuned the framework on the VCR dataset. Li *et al.* [16] proposed a cross-modal contrastive learning method to learn better alignment of cross-modal data. With regard to graph representation and learning, several methods [8], [9], [17] were investigated on the VCR task. Yu *et al.* [9] built answer-vision and answer-question heterogeneous graphs for networks to do reasoning. Wu *et al.* [17] developed visual neuron connectivity to build visual graph with linguistic data considered for graph convolutional networks to learn. Zhang *et al.* [8] constructed visual and linguistic graphs respectively, and then fused them for cross-modal reasoning. These methods all focused on visual features of objects and ignored their exact spatial representations and relationships, which also have influence on correctly understanding on visual interactive features. In this work, image depth is introduced into VCR, enhancing visual features with pseudo 3D position and depth image features. Then, depth differences are used to guide the attention mechanism originally based on semantic similarities.

### B. Depth Estimation

Depth estimation from images is an important task in computer vision, which is widely used in simultaneous localization and mapping (SLAM) [18], object detection [19] and semantic segmentation [20]. Depth estimation can be divided into binocular depth estimation [21] and monocular depth estimation [12]. Compared with the binocular camera system, the monocular camera system is more convenient and inexpensive to be deployed. Therefore, monocular depth estimation is easier to be applied to other tasks. Zhang *et al.* [18] presented a dynamic visual SLAM system tracking both poses and bounding boxes of dynamic object, where dynamic features were fetched by monocular depth estimation. Cao *et al.* [19] encoded structure correlations from monocular depth data, and embeded them with appearance information learnt from RGB data. Ergul *et al.* [20] proposed to fuse the 3D geometric structure of the scene into the segmentation based on depth maps estimated from one single image via a monocular depth estimation model. All works above used

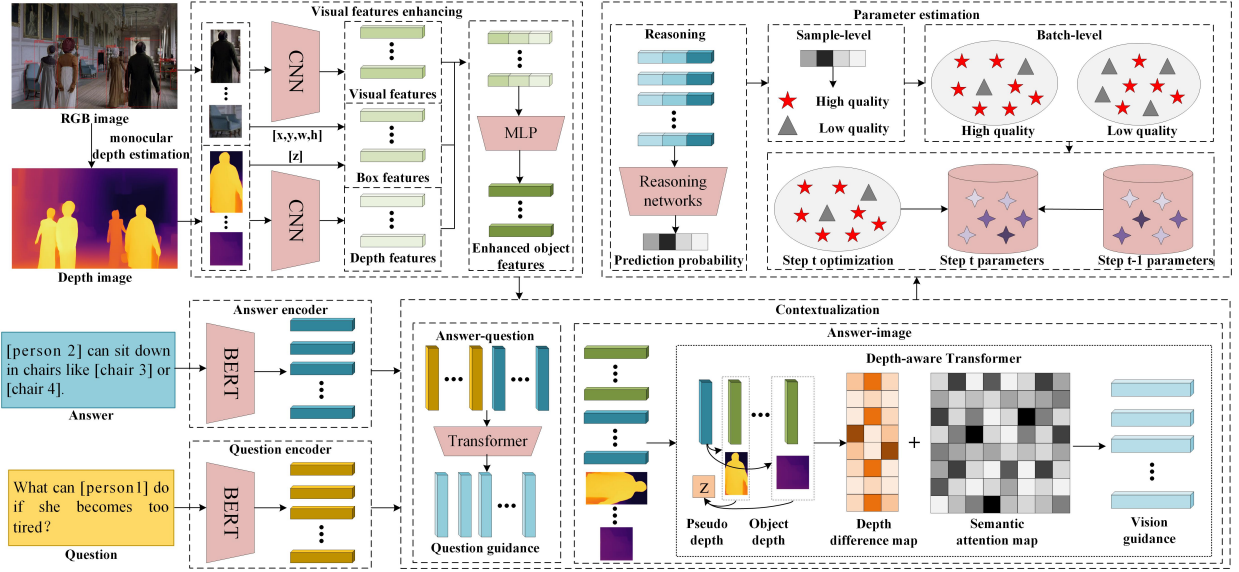


Fig. 2. Illustration of the proposed PPTMCO architecture. The framework consists of three key parts: (1) visual features enhancing, (2) answer-image contextualization by depth-aware Transformer, and (3) parameter estimation by reasoning confidence.

depth images to assist pure visual task, and few efforts were devoted to more complicated cross-modal tasks. In this paper, depth images are investigated in the cross-modal VCR task, where visual data need to further interact with linguistic data to realize image understanding.

### III. PROPOSED PPTMCO

In this section, the overview of the proposed framework is firstly introduced. Then, visual features enhancing with image depth, depth-aware Transformer for answer-image association, and parameter estimation method guided by multi-level reasoning confidence are described in detail.

#### A. Overview

The VCR task is to choose an answer and further provide a rationale justifying based on the given image and question, which consists of the following three subtasks:

- 1)  $Q \rightarrow A$ : Given an image and a question, the model should choose the right option from four answers.
- 2)  $QA \rightarrow R$ : Given an image, a question and the correct answer, the model should choose the right option from four rationales.
- 3)  $Q \rightarrow AR$ : Given an image and a question, the model should choose both the right answer and rationale.

To do  $Q \rightarrow AR$ , the frameworks need to both do  $Q \rightarrow A$  and  $QA \rightarrow R$ , which can be viewed as two four-way classification problems. The results of  $Q \rightarrow AR$  can be obtained by combining the results of  $Q \rightarrow A$  and  $QA \rightarrow R$ .

The architecture of the proposed PPTMCO framework is illustrated in Fig. 2. The image regions, question and answer data are firstly fed into pre-trained networks to extract features. Then, original visual features are enhanced by image depth features along with pseudo 3D positions. The framework utilizes plain Transformer and depth-aware Transformer to do

answer-question and answer-image contextualization, respectively. Finally, model parameters are estimated by weightedly integrating multiple sets of parameters based on multi-level reasoning confidence.

#### B. Visual Feature Enhancing with Image Depth

Given a question with  $N_q$  words  $U_q = \{u_i^q\}_{i=1}^{N_q}$  or a answer with  $N_a$  words  $U_a = \{u_i^a\}_{i=1}^{N_a}$ , the linguistic features of the question  $T_q = \{t_i^q\}_{i=1}^{N_q}$  or those of the answer  $T_a = \{t_i^a\}_{i=1}^{N_a}$  are obtained by a pre-trained BERT and a subsequent bidirectional LSTM. Visual features are enhanced by pseudo 3D positions and depth image features.

Given  $N_o$  objects  $O = \{o_i\}_{i=1}^{N_o}$  in a RGB image  $I$ , the original visual features  $S = \{s_i\}_{i=1}^{N_o}$ ,  $s_i \in \mathbb{R}^d$  are extracted by a pre-trained CNN, where  $d$  is the feature dimension. The depth image  $I_D$  is generated via the monocular depth estimation model [12] applied on the original RGB image  $I$ . Each object  $o_i$  corresponds to a bounding box denoted as  $(x_i, y_i, w_i, h_i)$ , where  $x_i, y_i$  represent the 2D coordinates of the box center and  $w_i, h_i$  represent the width and height of the box in the image. The depth image is aligned with the RGB image, and the bounding box can also be used to indicate the 2D position of the object in the depth image. Since the object is typically in the center of the bounding box with a few irrelevant pixels on the edge, the pixel value  $z_i$  at the position of box center  $(x_i, y_i)$  in the depth image is used as the depth coordinate of the object. Then, the pseudo 3D position feature is characterized by the box feature  $s_i^{box}$  consisting of six elements as

$$s_i^{box} = [x_i, y_i, z_i, w_i, h_i, w_i * h_i], \quad (1)$$

where  $x_i, y_i, z_i, w_i, h_i$  are all normalized in range  $[0, 1]$ .

To integrate depth information more accurately, a typical CNN is applied on the box region of the depth image to obtain the depth feature  $s_i^{depth} \in \mathbb{R}^d$  of the object. The enhanced



object feature  $s_i^e \in \mathbb{R}^d$  is jointly learnt from  $s_i, s_i^{box}, s_i^{depth}$ , which can be formulated as

$$s_i^e = fc(\text{concat}([s_i, s_i^{box}, s_i^{depth}])), \quad (2)$$

where  $fc(\cdot)$  is a fully-connected layer, and  $\text{concat}$  is the concatenating operator. The enhanced object feature with exact spatial information can more sufficiently represent the object, and provide spatial positional encoding for cross-modal Transformer in analogy with sequential positional encoding in plain Transformer.

### C. Depth-aware Transformer

After obtaining visual and linguistic features, the framework adopts Transformer-based models to associate them with each other. Plain Transformer model is used in the answer-question branch while depth-aware Transformer is proposed in the answer-image branch.

Given a sequence  $X = \{x_i\}_{i=1}^n$  for a plain Transformer layer, the attention mechanism can be formulated as

$$A = \frac{Q \cdot (K)^T}{\sqrt{d}}, \quad (3)$$

where  $A \in \mathbb{R}^{n \times n}$  represents the attention weight matrix, and  $Q_i, K_i$  are projections of  $x_i$  using independent fully-connected layers. In the answer-image branch, the sequence for depth-aware Transformer is composed of objects and answer words as  $\{s_1, \dots, s_{N_o}, t_1, \dots, t_{N_a}\}$ .

**Depth-aware attention between objects.** The plain attention mechanism is mainly based on semantic similarities. However, two objects with similar visual appearances and quite different depth values may have discriminative semantic relationships with another object. As is assumed that objects with similar depth values are more likely to have close relationships, depth differences are used to guide the attention mechanism in depth-aware Transformer, following the principle that the more similar the depth is, the more attention need be paid. With regard to objects  $i, j$ , depth difference can be calculated as

$$\Delta z_{ij} = |z_i - z_j| \quad (4)$$

where  $\Delta z_{ij} \in [0, 1]$ . To design the attention mechanism as the principle above,  $b_{ij}$  is proposed to adjust the semantic attention weights by  $\Delta z_{ij}$ , which is formulated as

$$b_{ij} = |A_{ij}| * (e^{-\Delta z_{ij}} - \alpha), \quad (5)$$

where adjust matrix  $b_{ij}$  grows from negative to positive in the scale of  $|A_{ij}|$  as  $\Delta z_{ij}$  declines, and  $\alpha$  is the depth bias. The depth-aware attention weight is calculated as follow:

$$A_{ij}^{depth} = A_{ij} + b_{ij} \quad (6)$$

**Depth-aware attention from words to objects.** The answer is a description related to objects in the image. For an word in the answer, it is mainly associated with objects in a level of depth. Therefore, the word implicitly corresponds to a depth level, which is reflected by a pseudo depth value given in depth-aware Transformer. The pseudo depth  $\tilde{z}_i$  of the word  $i$  based on objects is calculated as follow:

$$\tilde{z}_i = \sum \text{softmax}(A_{ij}) * z_j \quad (N_o < j \leq N_o + N_a) \quad (7)$$

Therefore, with regard to a word  $i$  and an object  $j$ , depth difference can also be obtained by

$$\Delta z_{ij} = |\tilde{z}_i - z_j|. \quad (8)$$

The depth-aware attention mechanism from words to objects can be integrated into the unified framework in a way similar as Eq. (5) and (6).

### D. Parameter Estimation Guided by Multi-level Reasoning Confidence

After contextualizing answer words with image regions and question words, the vision-guidance answer word representation  $T_{ai} \in \mathbb{R}^{N_a \times d}$  and the question-guidance answer word representation  $T_{aq} \in \mathbb{R}^{N_a \times d}$  are selected for further reasoning, which are concatenated with the original answer word representation  $T_a$  to obtain the sequential reasoning feature  $T_a^{reason} \in \mathbb{R}^{N_a \times 3d}$  as

$$T_a^{reason} = \text{concat}([T_a, T_{ai}, T_{aq}]). \quad (9)$$

The sequential reasoning feature is required to be pooled as a vector for the classification network, which is a two-layer fully-connected network adopted in [7], [8], [10] as well. The output is activated by softmax function to obtain the prediction probability for four choices  $P = [p_1, p_2, p_3, p_4]$ .

The framework is trained to optimize parameters on mini-batches. For such a challenging reasoning task with diverse samples, an optimization is probable to lead to a sub-optimized direction for the barely satisfactory reasoning performance on the mini-batch, especially at a later stage of training. Therefore, selectively using multiple sets of parameters to estimate parameters can relieve the stochastic optimization problem on a mini-batch.

Here, according to the sample-level and batch-level reasoning confidence, an optimization is divided into high-quality and low-quality. Given a batch with  $N_b$  samples, predictions on the batch can be denoted as  $\{P_i\}_{i=1}^{N_b}$ .

**Sample-level high-quality:** The sample is predicted correctly with high-confidence denoted as  $\max(P_i) > c_{sample}$ .

**Batch-level high-quality:** The proportion of high-quality reasoning samples in the batch is high denoted as  $N_{sample\_h}/N_b > c_{batch}$ , and the prediction accuracy of the optimization is better than the previous one.  $N_{sample\_h}$  is the number of high-quality reasoning samples in the batch.

Parameters estimated  $K_t^{es}$  are updated as the training step  $t$ . To ensure the continuity of the optimization, optimization on the high-quality reasoning batch and that on the low-quality one are weightedly integrated by  $\beta$ , where  $\beta$  equals 1 for high-quality one and  $N_{sample\_h}/N_b$  for low-quality one. Parameters estimated  $K_t^{es}$  at the step  $t$  are generated based on parameters optimized this time and parameters estimated at the previous step  $t-1$  as follow:

$$K_t^{es} = \beta * (1 - \gamma) * K_t + (1 - \beta * (1 - \gamma)) * K_{t-1}^{es}, \quad (10)$$

where  $\gamma$  is the hyperparameter controlling the number of steps for integrating.

### E. Implementation

The proposed framework is implemented on PyTorch and trained with 4 Tesla V100 GPUs. The models for the subtasks  $Q \rightarrow A$  and  $QA \rightarrow R$  possess identical architecture with their weights trained separately. The prediction for the subtask  $Q \rightarrow AR$  is the combination of the predictions for  $Q \rightarrow A$  and  $QA \rightarrow R$ . In the stage of feature extraction for original visual and linguistic data, each object in the given image is extracted as a 512-dimensional vector by the method in [10] with ResNet101 [22] as the backbone. Each word is embedded as a 768-dimensional feature by a pre-trained BERT [23], and sequential words as a whole sentence are further input into a single-layer bidirectional LSTM model to obtain 512-dimensional vectors for each word. The CNN networks used for depth images have three convolutional layers, and a fully-connected layer to generate 512-dimensional vectors. The visual features enhanced are also 512-dimensional. The dropout rate is 0.3 in Bi-LSTM and 0.1 in Transformer. The parameters of Transform-based model are trained by Noam [13] while the remaining modules are trained by Adam [24] with the learning rate initialized as 0.0002.  $\alpha$  in depth-aware Transformer is set as 0.6, and  $\gamma$  in PEMRC is set as 0.9998.  $c_{sample}$  and  $c_{batch}$  are 0.55 and 0.6. The batch size is 96, and the model is trained for 30 epochs with early stopping.

## IV. EXPERIMENT

### A. Dataset

Extensive experiments are carried out on the VCR benchmark dataset [7], which is composed of 290k four-way multiple-choice QA problems derived from 110k movie scenes. Different from VQA dataset where the answer is usually a single word, the answer and rationale in the VCR dataset is more complicated and in the form of mixtures of visual and linguistic words. The average lengths of the answers and rationales are over 7.5 words and 16 words, respectively. Following the data partition practice [7], the training set consists of 80,418 images with 212,923 questions, the validation set is composed of 9,929 images with 26,534 questions.

### B. Evaluation Metric and Baseline

The evaluation metric is classification accuracy, which is a ratio of correctly classified samples to all test samples. The competing methods are divided into three categories: (1) text-only baselines, including BERT [23], BERT (response only) [23], ESIM+ELMO [25] and LSTM+ELMO [25], which don't utilize visual information and can be used to evaluate the influence of visual context; (2) VQA baselines, including RevisitedVQA [26], BottomUpTopDown [27], MLB [28] and MUTAN [29], which are originally designed for VQA and modified to perform VCR (compared with these methods, the capability of the proposed framework to model the correlation between the complex response and the question or image can be evaluated); (3) VCR methods, including R2C [7], CKRM [14], TAB-VCR [10], CCN [17], HGL [9], ECMR [8], VC R-CNN [30], CL-VCR [31], MCC [11] and JAE [32].

The brief descriptions of the competing VCR methods are presented below. **R2C** adopts bilinear attention mechanism and

LSTM to associate image with text for reasoning. **CKRM** is an attention-based model to transfer external knowledge into the VCR task. **TAB-VCR** integrates attribute information into visual features and assigns extra tags to image grounding for the VCR task. **CCN** employs a connective cognition network and reorganizes visual neuron connectivity to do VCR. **HGL** operates heterogeneous graph learning based on the cross-modal correlation between image and text. **ECMR** integrates visual graph and linguistic graph for cross-modal reasoning. **VC R-CNN** employs region-based CNN to perform causal intervention for visual feature enhancement. **CL-VCR** adopts a curriculum-based masking approach to training model more robustly for VCR. **MCC** generates counterfactual samples and uses a contrastive learning strategy to train VCR framework. **JAE** presents a plug-and-play knowledge distillation enhanced framework to do VCR.

### C. Quantitative Result

The quantitative results achieved by the proposed PPTMCO compared with several competing methods for the three subtasks in VCR are given in Table I. With regard to these text-only baselines, performances are bad without considering the important visual information. These VQA baselines gain improvements compared with text-only baselines, but still cannot achieve satisfactory results since the expressions in VCR are more complicated. For the VCR methods, TAB-VCR [10], ECMR [8], and MCC [11] adopting visual features integrating attributes achieve better performances in general compared with other baselines R2C [7], CKRM [14], CCN [17], HGL [9] using plain visual features. Further considering exact 3D positions via image depth, the proposed PPTMCO framework obtains the best performance with 72.2% for the  $Q \rightarrow A$  task, 73.8% for the  $QA \rightarrow R$  task, 53.5% for the  $Q \rightarrow AR$  task on the validation set, respectively. In comparison to MCC [11] where the framework is trained via counterfactual samples and contrastive learning, the proposed PPTMCO adopts a parameter estimation method guided by multi-level reasoning confidence to optimize the framework. As a result, PPTMCO gains the improvements of 0.5% for the  $Q \rightarrow AR$  task on the validation set over MCC. As for the VC R-CNN [30] method using causal intervention, the CL-VCR [31] method with robust training, and JAE [32] adopting knowledge distillation, the proposed PPTMCO has superiority as well. All the above results demonstrate the effectiveness of the proposed PPTMCO.

### D. Ablation Study

To evaluate the effectiveness of the visual feature enhancing (VFE), DT and PEMRC modules in the framework, several models are designed to do ablation study as follows.

**Base.** A variant of the R2C model [7] replaces the backbone with ResNet101, and uses plain Transformer to do contextualization and reasoning instead of LSTM.

**Base+visual features enhanced with 2D positions (VFE2D).** A variant of the base model uses the visual features enhanced by 2D positions obtained in the

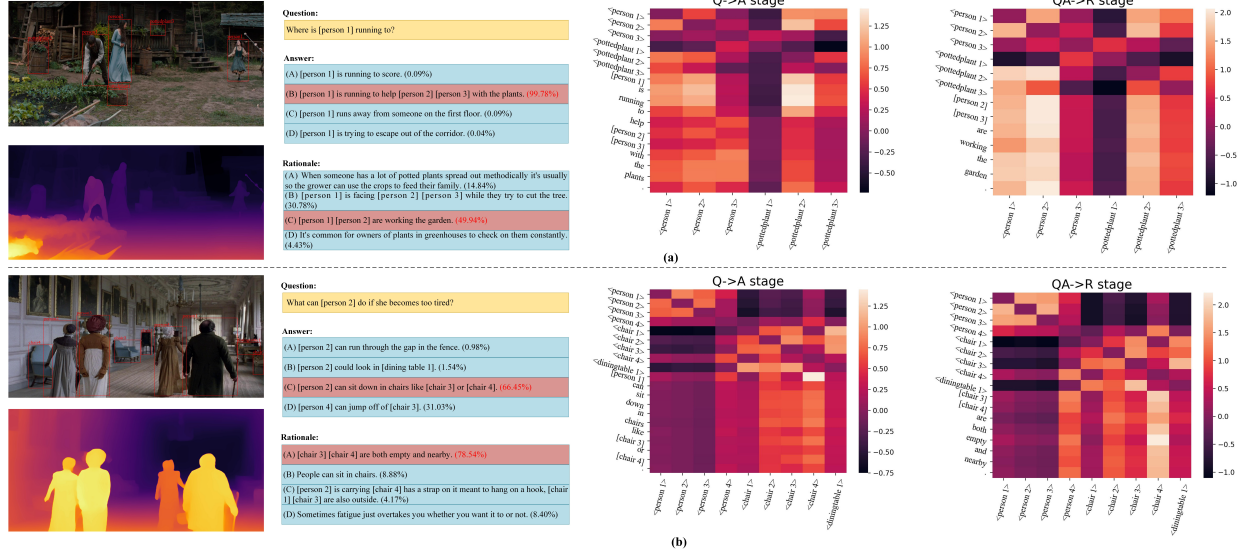


Fig. 3. Instances of successful cases for the VCR task obtained by the proposed PPTMCO. The percentages in brackets are the probabilities predicted by PPTMCO, and the choices filled in brown are ground-truths. To be distinguishable,  $\langle person\ 1 \rangle$  means visual object,  $[person1]$  means linguistic entity. The heatmaps for the ground-truth choices on the right indicate the final adjustment matrix for answer-image contextualization.

TABLE I  
COMPARISON OF ACCURACY FOR THREE SUBTASKS IN VCR ACHIEVED BY THE COMPETING METHODS ON THE VALIDATION SET OF VCR DATASET.

| Methods                   | $Q \rightarrow A$ | $QA \rightarrow R$ | $Q \rightarrow AR$ |
|---------------------------|-------------------|--------------------|--------------------|
| BERT [23]                 | 53.8              | 64.1               | 34.8               |
| BERT (response only) [23] | 27.6              | 26.3               | 7.6                |
| ESIM+ELMO [25]            | 45.8              | 55.0               | 25.3               |
| LSTM+ELMO [25]            | 28.1              | 28.7               | 8.3                |
| RevisitedVQA [26]         | 39.4              | 34.0               | 13.5               |
| BottomUpTopDown [27]      | 42.8              | 25.1               | 10.7               |
| MLB [28]                  | 45.5              | 36.1               | 17.0               |
| MUTAN [29]                | 44.4              | 32.0               | 14.6               |
| R2C [7]                   | 63.8              | 67.2               | 43.1               |
| CKRM [14]                 | 66.2              | 68.5               | 45.6               |
| TAB-VCR [10]              | 69.9              | 72.2               | 50.6               |
| CCN [17]                  | 67.4              | 70.6               | 47.7               |
| HGL [9]                   | 69.4              | 70.6               | 49.1               |
| ECMR [8]                  | 70.7              | 72.0               | 51.1               |
| MCC [11]                  | 71.7              | 73.4               | 52.9               |
| JAIE [32]                 | 70.5              | 73.1               | 51.8               |
| VC R-CNN [30]             | 67.4              | 69.5               | -                  |
| CL-VCR [31]               | 69.9              | 70.6               | -                  |
| PPTMCO                    | <b>72.2</b>       | <b>73.8</b>        | <b>53.5</b>        |

TABLE II  
ABLATION STUDY ON THE VALIDATION SET FOR THREE SUBTASKS IN VCR.

| Models                     | $Q \rightarrow A$ | $QA \rightarrow R$ | $Q \rightarrow AR$ |
|----------------------------|-------------------|--------------------|--------------------|
| Base                       | 70.2              | 71.6               | 50.5               |
| Base+VFE2D                 | 70.6              | 72.1               | 51.1               |
| Base+VFE                   | 71.2              | 72.6               | 51.9               |
| Base+VFE+DT                | 71.7              | 73.2               | 52.7               |
| Base+VFE+DT+PEMRC (PPTMCO) | <b>72.2</b>       | <b>73.8</b>        | <b>53.5</b>        |

RGB image, which is to evaluate the effect of 2D object positions.

**Base+VFE.** A variant model of PPTMCO only adopts the visual features enhanced by pseudo 3D positions and depth image features. This model is utilized to evaluate the effect of image depth.

**Base+VFE+DT.** A variant model of PPTMCO leverages VFE and DT to evaluate the effectiveness of attention mechanism guided by depth difference.

**Base+VFE+DT+PEMRC.** The proposed PPTMCO model incorporates VFE, DT and PEMRC.

The ablation study results for the three subtasks in VCR are shown in Table II. As can be observed, *Base+VFE2D* obtains the improvements of 0.4% for the  $Q \rightarrow A$  task, 0.5% for the  $QA \rightarrow R$  task, and 0.6% for the  $Q \rightarrow AR$  task

on the validation set respectively, indicating the importance of object positions for image understanding. With depth information considered, *Base+VFE* further gains improvements since pseudo 3D positions are more exact. Compared with *Base+VFE*, *Base+VFE+DT* adopting depth differences to guide attention mechanism achieves better performances of 0.5%, 0.6% and 0.8% improvements for the three subtasks, indicating that depth differences focus the model to pay more attention to the objects in the related depth level. The proposed *PPTMCO* utilizes PEMRC to optimize parameters and obtains the best performance on the validation set.

### E. Visualization and Analysis

Instances of successful cases obtained by the proposed PPTMCO are shown in Fig. 3. As can be seen in Fig. 3(a), correlation between irrelevant  $\langle person\ 1 \rangle$  and  $\langle pottedplant\ 1 \rangle$  is weakened in the adjustment matrix guided by depth differences. The answer and rational both capture the depth level of  $\langle person\ 1 \rangle$ ,  $\langle person\ 2 \rangle$ ,  $\langle person\ 3 \rangle$ ,  $\langle pottedplant\ 2 \rangle$ . In Fig. 3(b), the answer and rational both pay more attention to closer  $\langle chair\ 2 \rangle$ ,  $\langle chair\ 3 \rangle$ ,  $\langle chair\ 4 \rangle$  instead of  $\langle chair\ 1 \rangle$  on the basis of understanding the sentence. Therefore, the proposed PPTMCO can properly focus on key cues. Since models for  $Q \rightarrow A$  and  $QA \rightarrow R$  are trained respectively, elements

in adjustment matrices from words to objects appear similar, which also demonstrates the stability of the depth difference guidance.

## V. CONCLUSION

Visual commonsense reasoning is a challenging task since it is difficult to sufficiently understand the image and properly associate it with linguistic data. In this paper, a framework named PPTMCO is proposed to achieve more discriminative visual features and use image depth differences to assist associating between cross-modal data. Specifically, image depth is introduced to represent pseudo 3D positions of objects along with 2D coordinates in the image and further enhance visual features. Depth-aware Transformer is proposed to do attention mechanism with depth differences to guide from answer words and objects to objects, where each word is tagged with pseudo depth value according to related objects. Considering samples of VCR varying from each other and difficulty to be fit, a model parameter estimation method is further proposed to weightedly integrate parameters optimized by mini-batches based on multi-level reasoning confidence. The experiments conducted on the benchmark VCR dataset demonstrate the effectiveness of the proposed method.

## REFERENCES

- [1] H. Shi, H. Li, Q. Wu, and K. N. Ngan, "Query reconstruction network for referring expression image segmentation," *IEEE Trans. Multimedia*, vol. 23, pp. 995–1007, Apr. 2020.
- [2] J. Zhu and H. Wang, "Multi-scale conditional relationship graph network for referring relationships in images," *IEEE Trans. Cogn. Dev. Syst.*, vol. 14, no. 2, pp. 752–760, Jun. 2022.
- [3] L. Yang, H. Wang, P. Tang, and Q. Li, "Captionnet: A tailor-made recurrent neural network for generating image descriptions," *IEEE Trans. Multimedia*, vol. 23, pp. 835–845, Apr. 2020.
- [4] H. Wang, P. Tang, Q. Li, and M. Cheng, "Emotion expression with fact transfer for video description," *IEEE Trans. Multimedia*, vol. 24, pp. 715–727, Feb. 2022.
- [5] W. Guo, Y. Zhang, J. Yang, and X. Yuan, "Re-attention for visual question answering," *IEEE Trans. Image Process.*, vol. 30, pp. 6730–6743, Jul. 2021.
- [6] H. Zhong, J. Chen, C. Shen, H. Zhang, J. Huang, and X.-S. Hua, "Self-adaptive neural module transformer for visual question answering," *IEEE Trans. Multimedia*, vol. 23, pp. 1264–1273, May 2020.
- [7] R. Zellers, Y. Bisk, A. Farhadi, and Y. Choi, "From recognition to cognition: Visual commonsense reasoning," in *Proc. CVPR'19*, Jun. 2019, pp. 6713–6724.
- [8] X. Zhang, F. Zhang, and C. Xu, "Explicit cross-modal representation learning for visual commonsense reasoning," *IEEE Trans. Multimedia*, vol. 24, pp. 2986–2997, 2022.
- [9] W. Yu, J. Zhou, W. Yu, X. Liang, and N. Xiao, "Heterogeneous graph learning for visual commonsense reasoning," in *Proc. NeurIPS'19*, Dec. 2019, pp. 2769–2779.
- [10] J. Lin, U. Jain, and A. G. Schwing, "Tab-vcr: Tags and attributes based vcr baselines," in *Proc. NeurIPS'19*, Dec. 2019, pp. 15 615–15 628.
- [11] X. Zhang, F. Zhang, and C. Xu, "Multi-level counterfactual contrast for visual commonsense reasoning," in *Proc. ACM MM'21*, Oct. 2021, pp. 1793–1802.
- [12] R. Ranftl, A. Bochkovskiy, and V. Koltun, "Vision transformers for dense prediction," in *Proc. CVPR'21*, Jun. 2021, pp. 12 179–12 188.
- [13] A. Vaswani, N. Shazeer, N. Parmar, J. Uszkoreit, L. Jones, A. N. Gomez, E. Kaiser, and I. Polosukhin, "Attention is all you need," in *Proc. NeurIPS'17*, Dec. 2017, pp. 5998–6008.
- [14] Z. Wen and Y. Peng, "Multi-level knowledge injecting for visual commonsense reasoning," *IEEE Trans. Circuits Syst. Video Technol.*, vol. 31, no. 3, pp. 1042–1054, May 2020.
- [15] W. Su, X. Zhu, Y. Cao, B. Li, L. Lu, F. Wei, and J. Dai, "Vi-bert: Pre-training of generic visual-linguistic representations," in *Proc. ICLR'20*, Apr. 2020.
- [16] W. Li, C. Gao, G. Niu, X. Xiao, H. Liu, J. Liu, H. Wu, and W. Haifeng, "Unimo: Towards unified-modal understanding and generation via cross-modal contrastive learning," in *Proc. ACL'21*, Aug. 2021, pp. 2592–2607.
- [17] A. Wu, L. Zhu, Y. Han, and Y. Yang, "Connective cognition network for directional visual commonsense reasoning," in *Proc. NeurIPS'19*, Dec. 2019, pp. 5669–5679.
- [18] H. Zhang, H. Uchiyama, S. Ono, and H. Kawasaki, "Motslam: Mot-assisted monocular dynamic slam using single-view depth estimation," in *arXiv:2210.02038*, Oct. 2022.
- [19] Y. Cao, H. Zhang, Y. Li, C. Ren, and C. Lang, "Cman: Learning global structure correlation for monocular 3d object detection," *IEEE Trans. Intell. Transp. Syst. (Early access)*, pp. 1–11, 2022.
- [20] M. Ergül and A. Alatan, "Depth is all you need: Single-stage weakly supervised semantic segmentation from image-level supervision," in *Proc. ICIIP'22*, Oct. 2022, pp. 4233–4237.
- [21] A. Pilzer, S. Lathuilière, D. Xu, M. M. Puscas, E. Ricci, and N. Sebe, "Progressive fusion for unsupervised binocular depth estimation using cycled networks," *IEEE Trans. Pattern Anal. Mach. Intell.*, vol. 42, no. 10, pp. 2380–2395, Oct. 2020.
- [22] K. He, X. Zhang, S. Ren, and J. Sun, "Deep residual learning for image recognition," in *Proc. CVPR'16*, Jun. 2016, pp. 770–778.
- [23] J. Devlin, M.-W. Chang, K. Lee, and K. Toutanova, "Bert: Pre-training of deep bidirectional transformers for language understanding," in *Proc. NAACL'19*, Jun. 2019, pp. 4171–4186.
- [24] D. P. Kingma and J. Ba, "Adam: A method for stochastic optimization," in *Proc. ICLR'14*, Apr. 2014.
- [25] Q. Chen, X. Zhu, Z.-H. Ling, S. Wei, H. Jiang, and D. Inkpen, "Enhanced lstm for natural language inference," in *Proc. ACL'17*, Jul. 2017, pp. 1657–1668.
- [26] A. Jabri, A. Joulin, and L. Van Der Maaten, "Revisiting visual question answering baselines," in *Proc. ECCV'16*, Oct. 2016, pp. 727–739.
- [27] P. Anderson, X. He, C. Buehler, D. Teney, M. Johnson, S. Gould, and L. Zhang, "Bottom-up and top-down attention for image captioning and visual question answering," in *Proc. CVPR'18*, Jun. 2018, pp. 6077–6086.
- [28] J.-H. Kim, K.-W. On, W. Lim, J. Kim, J.-W. Ha, and B.-T. Zhang, "Hadamard product for low-rank bilinear pooling," in *Proc. ICLR'17*, Nov. 2017.
- [29] H. Ben-Younes, R. Cadene, M. Cord, and N. Thome, "Mutan: Multi-modal tucker fusion for visual question answering," in *Proc. CVPR'17*, Jun. 2017, pp. 2612–2620.
- [30] T. Wang, J. Huang, H. Zhang, and Q. Sun, "Visual commonsense r-cnn," in *Proc. CVPR'20*, Jun. 2020, pp. 10 757–10 767.
- [31] K. Ye and A. Kovashka, "A case study of the shortcut effects in visual commonsense reasoning," in *Proc. AAAI'21*, Feb. 2021, pp. 3181–3189.
- [32] Z. Li, Y. Guo, K. Wang, Y. Wei, L. Nie, and M. Kankanhalli, "Joint answering and explanation for visual commonsense reasoning," in *arXiv:2202.12626*, Feb. 2022.